AD-A069 963 NAVAL RESEARCH LAB WASHINGTON DC F/G 20/6
MODEL FOR PREDICTING RELATIVE SIGNAL POWER IN COHERENT ANTI-STO--ETC(U)
APR 79 W S SANDERS

UNCLASSIFIED NRL-MR-3973 NL

1 OF 1
AD A069963

END
DATE FILMED
7-79
DDC

(12) LEVEL II

NRL Memorandum Report 3973

Model for Predicting Relative Signal Power in Coherent Anti-Stokes Raman Spectroscopy

WILLIAM A. SANDERS

Chemistry Division

April 20, 1979

NAVAL RESEARCH LABORATORY
Washington, D.C.

(9) Memorandum rept.,

SECURITY CLASSIFICATION OF THIS PAGE (When Data Entered)

REPORT DOCUMENTATION PAGE

READ INSTRUCTIONS BEFORE COMPLETING FORM

1. REPORT NUMBER: NRL Memorandum Report 3973
2. GOVT ACCESSION NO.
3. RECIPIENT'S CATALOG NUMBER

4. TITLE (and Subtitle): (6) MODEL FOR PREDICTING RELATIVE SIGNAL POWER IN COHERENT ANTI-STOKES RAMAN SPECTROSCOPY
5. TYPE OF REPORT & PERIOD COVERED: Interim report on a continuing NRL problem.
6. PERFORMING ORG. REPORT NUMBER

7. AUTHOR(s): (10) William A. Sanders *
8. CONTRACT OR GRANT NUMBER(s): (14) 20 Apr 79

9. PERFORMING ORGANIZATION NAME AND ADDRESS: Naval Research Laboratory, Washington, DC 20375 (12) 46 p.
10. PROGRAM ELEMENT, PROJECT, TASK AREA & WORK UNIT NUMBERS: NRL Problem C07-16.101, Project 61153N-13

11. CONTROLLING OFFICE NAME AND ADDRESS: (14) NRL-MR-3973
12. REPORT DATE: April 20, 1979
13. NUMBER OF PAGES: 45

14. MONITORING AGENCY NAME & ADDRESS(if different from Controlling Office)
15. SECURITY CLASS. (of this report): UNCLASSIFIED
15a. DECLASSIFICATION/DOWNGRADING SCHEDULE

16. DISTRIBUTION STATEMENT (of this Report)

Approved for public release; distribution unlimited.

17. DISTRIBUTION STATEMENT (of the abstract entered in Block 20, if different from Report)

18. SUPPLEMENTARY NOTES

*Permanent address: Department of Chemistry, The Catholic University of America, Washington, DC 20064

19. KEY WORDS (Continue on reverse side if necessary and identify by block number)

Nonlinear optics
Raman
Spectroscopy
CARS

20. ABSTRACT (Continue on reverse side if necessary and identify by block number)

A more general mathematical model has been developed for the prediction of signal power generated by the Coherent Anti-Stokes Raman Scattering process (CARS). Like previous treatments the model assumes that the laser beams have Gaussian profiles. However, provision is made for varying a number of experimental parameters, either singly or in combinations. In particular, the model allows for non-collinearity of the laser beams, different beam diameters, lateral offset of the beam centers, and relative displacement of the focal points of the beams.

(Continues)

DD FORM 1 JAN 73 1473 EDITION OF 1 NOV 65 IS OBSOLETE
S/N 0102-014-6601

251 950

JCB

20. Abstract (Continued)

Computational time requirements of the new model are not significantly greater than previous treatments of identical, collinear Gaussian beams, although the numerical integrations must be handled more carefully. Significant predictions of the model are:

1. Substantial power gains can be realized by tightening the focus of the ω_2 (dye laser) beam relative to the primary pumping beam.

2. Signal intensity is enhanced by a slight displacement of the focus of the ω_2 beam in the direction of propagation.

3. Substantial deviations from collinearity decrease the signal intensity sharply, but a small offset results in a slight enhancement.

4. Crossing the laser beams decreases the signal power, but the magnitude of the effect is smaller than might be expected.

5. The loss of signal power which results from a non-zero crossing angle can be compensated for (up to a crossing angle of about 1°) by introducing a small lateral offset.

6. For a typical set of experimental parameters, approximately 80% of the CARS power is generated in a region 1 cm long with its center at the beam focus.

CONTENTS

MODEL FOR PREDICTING RELATIVE SIGNAL POWER IN COHERENT ANTI-STOKES RAMAN SPECTROSCOPY

I. INTRODUCTION

With the current availability of versatile laser systems, there is increasing interest in higher-order Raman scattering techniques as tools for studying a wide variety of chemical systems (1). These methods have numerous advantages over conventional Raman spectroscopy, such as increased spatial resolution, greatly enhanced signal intensities, spatial filtering, etc. (2).

Typical of the higher-order Raman processes and one of the most promising from the standpoint of practical applications is the so-called coherent anti-Stokes Raman spectroscopy (CARS). In this case a sample is irradiated with two laser beams of frequency ω_1 and ω_2, and a signal corresponding to a characteristic Raman transition of the sample is generated at the frequency $\omega_3 = 2\omega_1 - \omega_2$. The signal is coherent and many times more intense than the corresponding output obtained by conventional Raman spectroscopy (3). An additional advantage is realized when the technique is applied to condensed phases in which there is a significant amount of dispersion. The phase-matching conditions of the

Note: Manuscript submitted February 8, 1979.

multi-photon process require that the two laser beams cross at a certain angle in the active region of the sample. The result is that the coherent signal emerges in a direction different from that of either of the two laser beams, and thus can be separated without the use of a monochromator. For gases the optimum crossing angle is near zero, so that spatial filtering can be achieved only by sacrificing signal intensity.

Theoretical calculations of CARS signal strengths in gaseous media have yielded very optimistic predictions of the ultimate sensitivity of the technique. The first rigorous treatment of the conversion process for collinear, focused Gaussian beams was carried out by Bjorklund (4). His calculations yielded results in general agreement with the experimental observations under the conditions of the mathematical model.

For realistic predictions of the optimum CARS performance under actual experimental conditions, a more general mathematical model is required. In a typical experiment the laser beams are not precisely collinear and do not have identical profiles. Furthermore, the beams may be deliberately crossed in a gaseous sample in order to achieve increased spatial resolution in the active region and spatial separation of the signal at the detector. It is important to know the extent to which performance is degraded when

the experimental parameters are varied away from the ideal case. Therefore, a more flexible predictive model would be of substantial value in selecting the optimum experimental conditions.

In this work the treatment of Bjorklund has been extended to include the effects of non-collinear, non-confocal beams with different profiles. In principle, the model is capable of dealing with arbitrarily large crossing angles between the two laser beams, but it has been applied only to the range of practical interest in gases ($\vartheta_c \lesssim 3^\circ$). Modifying the model to allow for the treatment of larger crossing angles would require additional algebraic manipulations, but would not increase the computational time significantly.

II. THE THEORETICAL MODEL

A. The General Case

In this section the most general experimental arrangement covered by the model is defined. All of the special cases considered below will be obtained from the general model by appropriate restrictions of the parameters.

Let us start with a laser beam of frequency ω_1 with propagation vector directed along the longitudinal axis of the sample cell (taken to be the z-axis). Assume the beam has a Gaussian profile (5), and assume it is focused inside the cell so that the electric field strength is given by

$$\vec{E}_1(\vec{r}) = \vec{E}_{10}\, e^{ik_1 z}\left(1 + i\frac{\mathcal{E}_1}{b_1}\right)^{-1} \exp\left[-\frac{k_1(x^2+y^2)}{b_1(1+i\mathcal{E}_1/b_1)}\right], \qquad (1)$$

where

$$b_1 = k_1 r_1^2 \qquad (2)$$

is a reduced form of the radius r_1 of the beam waist and

$$\mathcal{E}_1(z) = 2(z - f_1). \qquad (3)$$

The parameter f_1 is the z-coordinate of the beam waist. Without loss of generality, the origin of the coordinate system can be taken to be at the focus of the beam, so that

$$\mathcal{E}_1(z) = 2z \quad . \qquad (4)$$

Let the second laser beam have frequency ω_2 and propagation vector $\vec{k}_2$. The beam crossing geometry is shown in Figure 1. Note that the x-axis is chosen in such a way as to make both $\vec{k}_1$ and $\vec{k}_2$ parallel to the xz-plane. The y_2 axis is chosen to be parallel to the y-axis. The x_2z_2-plane cuts the y-axis at $y = y_c$, and the focus of the second beam ($z_2 = 0$) is displaced from the "crossing point" ($y = y_c$, $z = z_c$) by the distance d.

Assume the second beam is also a focused Gaussian. In the coordinate system (x_2, y_2, z_2) its electric field vector is given by

$$\vec{E}_2(\vec{r}) = \vec{E}_{20}\, e^{i\alpha} e^{i\vec{k}_2\cdot\vec{r}}\left(1 + \frac{i\mathcal{E}_2}{b_2}\right)^{-1} \exp\left[-\frac{k_2(x_2^2+y_2^2)}{b_2(1+i\mathcal{E}_2/b_2)}\right], \qquad (5)$$

where α is an arbitrary phase factor and all other

quantities have meanings which are analogous to the corresponding parameters in Eq. (1). For example,

$$\xi_2(z_2) = 2\,\Delta z_2 \ , \tag{6}$$

where Δz_2 is the distance between a particular point in space and the focus of the second beam, measured in the direction of $\vec{k}_2$. The focus of the second beam is assumed to lie in the plane $z_2 = 0$.

By making use of simple geometry, it is possible to express $E_2(\vec{r})$ in terms of the (x,y,z) coordinate system. The equations of the coordinate transformation are

$$x_2 = x\cos\vartheta_c - (z - z_c)\sin\vartheta_c \tag{7a}$$

$$y_2 = y - y_c \tag{7b}$$

$$z_2 = x\sin\vartheta_c + (z - z_c)\cos\vartheta_c - d \ , \tag{7c}$$

and the result is

$$\vec{E}_2(\vec{r}) = \vec{E}_{20}\, e^{i\alpha} \exp\left[i k_2 (x\sin\vartheta_c + z\cos\vartheta_c)\right]\left(1 + i\,\xi_2/b_2\right)^{-1}$$

$$\times \exp\left[-\frac{k_2}{b_2(1+i\,\xi_2/b_2)}\left\{\left[x\cos\vartheta_c - (z-z_c)\sin\vartheta_c\right]^2 + (y-y_c)^2\right\}\right] , \tag{8}$$

where

$$\xi_2(z) = 2x\sin\vartheta_c + 2(z-z_c)\cos\vartheta_c - 2d, \tag{9}$$

and $b_2 = k_2 r_2^2$ is the reduced radius of the ω_2 beam.

If it is assumed that both laser beams are polarized along the y-axis, then the polarization of the medium at the frequency $\omega_3 = 2\omega_1 - \omega_2$ is given by (6)

$$P_3(\vec{r}) = \frac{3}{4} N \chi(2\omega_1 - \omega_2) E_{10}^2 E_{20} e^{-i\alpha} b_1^2 b_2 e^{2ik_1 z}$$
$$\times \exp[-ik_2(x\sin\theta_c + z\cos\theta_c)](b_1 + i\xi_1)^{-2}(b_2 - i\xi_2)^{-1}$$
$$\times \exp[-2k_1(x^2+y^2)/(b_1+i\xi_1)]$$
$$\times \exp\left[-\frac{k_2}{b_2 - i\xi_2}\left\{[x\cos\theta_c - (z-z_c)\sin\theta_c]^2 + (y-y_c)^2\right\}\right] , \quad (10)$$

where N is the number density and $\chi(2\omega_1 - \omega_2)$ is the third-order polarizability of the medium at the frequency $2\omega_1 - \omega_2$. The Fourier transform of $P_3(\vec{r})$ is

$$P_3(\vec{K}) = (2\pi)^{-3}\int_{-\infty}^{\infty} dx' \int_{-\infty}^{\infty} dy' \int_{-\infty}^{\infty} dz' P_3(\vec{r}') e^{-i\vec{K}\cdot\vec{r}'} . \quad (11)$$

Assume

$$K_x, K_y \ll K_z \text{ and } |\vec{K}| - k_3 \ll |\vec{K}|, k_3 , \quad (12)$$

so that Kleinman's solution (7) to the wave equation is valid. These conditions are well-satisfied for laser beams at optical frequencies. Therefore, the Fourier components of the radiation generated in the active medium by the CARS process are given by

$$E_{3\vec{K}}(\vec{r}) = \frac{2\pi i k_0^2 z}{k_3} q(U_{\vec{K}}) e^{i\vec{K}\cdot\vec{r}} P_3(\vec{K}) , \quad (13)$$

where k_0 is the vacuum propagation number of the generated radiation and

$$q(U_{\vec{K}}) = \int_0^1 e^{-U_{\vec{K}} p}$$
$$= \int_0^1 \exp\left[-iz\left\{K_z - k_3 + \frac{K_x^2 + K_y^2}{2k_3}\right\}p\right] dp . \quad (14)$$

The total generated field at the frequency ω_3 is

obtained by substituting the expression for P (K), Eq. (11), into Eq. (13), using Eq. (14), and integrating over K:

$$E_3(\vec{r}) = \int_{-\infty}^{\infty} dK_x \int_{-\infty}^{\infty} dK_y \int_{-\infty}^{\infty} dK_z \, E_{3\vec{K}}(\vec{r}) \quad . \tag{15}$$

Defining

$$A' = \frac{3}{4} N \chi(2\omega_1 - \omega_2) E_{10}^2 E_{20} e^{-i\alpha} b_1^2 b_2 \quad , \tag{16}$$

we obtain

$$E_3(\vec{r}) = \frac{i k_0^2 z}{(2\pi)^2 k_3} A' \int_{-\infty}^{\infty} dK_x \int_{-\infty}^{\infty} dK_y \int_{-\infty}^{\infty} dK_z \int_0^1 \exp\left[-iz\left\{K_z - k_3 + \frac{K_x^2 + K_y^2}{2k_3}\right\}p\right] dp$$

$$\times e^{i\vec{K}\cdot\vec{r}} \int_{-\infty}^{\infty} dx' \int_{-\infty}^{\infty} dy' \int_{-\infty}^{\infty} dz' \exp\left[i\left\{(2k_1 - k_2\cos\vartheta_c)z' - k_2 \sin\vartheta_c x'\right\}\right]$$

$$\times \left\{b_1 + i\mathcal{E}_1(z')\right\}^{-2} \left\{b_2 - i\mathcal{E}_2(x', z')\right\}^{-1}$$

$$\times \exp\left[\frac{-2k_1(x'^2 + y'^2)}{b_1 + i\mathcal{E}_1(z')}\right] e^{-i\vec{K}\cdot\vec{r}'}$$

$$\times \exp\left[-\frac{k_2}{b_2 - i\mathcal{E}_2(x', z')}\left\{\left[x'\cos\vartheta_c - (z' - z_c)\sin\vartheta_c\right]^2 + (y' - y_c)^2\right\}\right] .$$

(17)

The first step is to integrate over K_z, using the relationship (8)

$$\int_{-\infty}^{\infty} e^{iaK_z} dK_z = 2\pi\delta(a) \quad , \tag{18}$$

to reduce the integral to the form

$$E_3(\vec{r}) = \frac{ik_0^2 z}{2\pi k_3} A' \int_{-\infty}^{\infty} dK_x \int_{-\infty}^{\infty} dK_y \int_0^1 \exp\left[-iz\left\{\frac{K_x^2 + K_y^2}{2k_3} - k_3\right\}p\right] dp$$

$$\times e^{iK_x(x-x')} e^{iK_y(y-y')} \int_{-\infty}^{\infty} dx' \int_{-\infty}^{\infty} dy' \int_{-\infty}^{\infty} dz' \, e^{-ik_2 \sin\vartheta_c x'}$$

$$\times e^{i(2k_1 - k_2\cos\vartheta_c)z'} \{b_1 + i\mathcal{E}_1(z')\}^{-2} \{b_2 - i\mathcal{E}_2(x', z')\}^{-1}$$

$$\times \exp\left[-\frac{2k_1(x'^2 + y'^2)}{b_1 + i\mathcal{E}_1(z')}\right] \delta[(1-p)z - z']$$

$$\times \exp\left[-\frac{k_2}{b_2 - i\mathcal{E}_2(x', z')}\left\{[x'\cos\vartheta_c - (z - z_2)\sin\vartheta_c]^2 + (y' - y_c)^2\right\}\right] . \tag{19}$$

The integration over z′ can then be carried out to yield

$$E_3(\vec{r}) = \frac{ik_0^2 z}{2\pi k_3} A' \int_{-\infty}^{\infty} dK_x \int_{-\infty}^{\infty} dK_y \int_0^1 dp \exp\left[-iz\left\{\frac{K_x^2 + K_y^2}{2k_3} - k_3\right\}p\right]$$

$$\times e^{iK_x(x-x')} e^{iK_y(y-y')} \int_{-\infty}^{\infty} dx' \int_{-\infty}^{\infty} dy' \, e^{-ik_2 \sin\vartheta_c x'}$$

$$\times \exp\left[i(2k_1 - k_2\cos\vartheta_c)(1-p)z\right] \left[b_1 + i\mathcal{E}_1\{(1-p)z\}\right]^{-2} \left[b_2 - i\mathcal{E}_2\{x', (1-p)z\}\right]^{-1}$$

$$\times \exp\left[-\frac{2k_1(x'^2 + y'^2)}{b_1 + i\mathcal{E}_1\{(1-p)z\}}\right] \exp\left[-\frac{k_2}{b_2 - i\mathcal{E}_2\{x', (1-p)z\}}\left\{[x'\cos\vartheta_c\right.\right.$$

$$\left.\left. - (z - zp - z_c)\sin\vartheta_c]^2 + (y' - y_c)^2\right\}\right] \tag{20}$$

Next, integrate over K_x and K_y, using the formula

$$\int_{-\infty}^{\infty} \exp[-iqx - isx^2]\,dx = \left(\frac{\pi}{is}\right)^{1/2} \exp\left(\frac{iq^2}{4s}\right), \tag{21}$$

to obtain

$$E_3(\vec{r}) = k_0^2 A' \exp[i(2k_1 - k_2\cos\vartheta_c)z] \int_0^1 dp \int_{-\infty}^{\infty} dx' \int_{-\infty}^{\infty} dy' \rho^{-1} e^{ik_3 zp}$$

$$\times e^{-ik_2 \sin\vartheta_c x'} \exp[-i(2k_1 - k_2\cos\vartheta_c)pz][b_1 + i\varepsilon_1\{(1-p)z\}]^{-2}$$

$$\times [b_2 - i\varepsilon_2\{x', (1-p)z\}]^{-1} \exp\left[\frac{ik_3 y'}{zp}\left(\frac{y'}{2} - y\right)\right]$$

$$\times \exp\left[-\frac{k_2}{b_2 - i\varepsilon_2\{x', (1-p)z\}}\left\{[x'\cos\vartheta_c - (z - zp - z_c)\sin\vartheta_c]^2 + y_c^2\right\}\right]$$

$$\times \exp\left[-\frac{2k_1 x'^2}{b_1 + i\varepsilon_1\{(1-p)z\}}\right] \exp\left[\frac{ik_3}{2zp}\{(x'-x)^2 + y^2\}\right]$$

$$\times \exp\left[-\frac{2k_1 y'^2}{b_1 + i\varepsilon_1\{(1-p)z\}} - \frac{k_2 y'^2}{b_2 - i\varepsilon_2\{x', (1-p)z\}}\right]$$

$$\times \exp\left[\frac{2k_2 y_c y'}{b_2 - i\varepsilon_2\{x', (1-p)z\}}\right] . \tag{22}$$

Finally, the integration over y' is carried out, also using

Eq. (21). The rather complicated expression which results can be simplified by defining

$$G_1(p) = b_1 + i\mathcal{E}_1\{(1-p)z\} = b_1 + 2i(1-p)z \tag{23}$$

and

$$G_2(x',p) = b_2 - i\mathcal{E}_2\{x', (1-p)z\} . \tag{24}$$

Then

$$E_3(\vec{r}) = \left(\frac{\pi}{i}\right)^{1/2} k_0^2 A' \exp\left[i(2k_1 - k_2\cos\vartheta_c)z\right]$$

$$\times \int_0^1 dp\, p^{-1} \exp\left\{\frac{ik_3}{2zp}(x^2+y^2)\right\} \exp\left[i(k_3 - 2k_1 + k_2\cos\vartheta_c)zp\right]$$

$$\times G_1(p)^{-2} \int_{-\infty}^{\infty} dx'\, e^{-ik_2\sin\vartheta_c x'} G_2(x',p)^{-1} \exp\left(-\frac{ik_3 x x'}{zp}\right)$$

$$\times \exp\left[\left(-\frac{2k_1}{G_1(p)} + \frac{ik_3}{2zp}\right)x'^2\right]\left[-\frac{2ik_1}{G_1(p)} - \frac{ik_2}{G_2(x',p)} - \frac{k_3}{2zp}\right]^{-1/2}$$

$$\times \exp\left[-\frac{k_2}{G_2(x',p)}\left\{\left[x'\cos\vartheta_c - (z - zp - z_c)\sin\vartheta_c\right]^2 + y_c^2\right\}\right]$$

$$\times \exp\left[\frac{i}{4}\left\{\frac{2ik_2 y_c}{G_2(x',p)} + \frac{k_3 y}{zp}\right\}^2\left\{-\frac{2ik_1}{G_1(p)} - \frac{ik_2}{G_2(x',p)} - \frac{k_3}{2zp}\right\}^{-1}\right] \tag{25}$$

Let

$$B_1(p) = \frac{2ik_1 p}{G_1(p)} + \frac{k_3}{2z} \quad , \tag{26}$$

so that

$$E_3(\vec{r}) = \left(\frac{\pi}{i}\right)^{1/2} k_0^2 A' e^{i(2k_1 - k_2)z} e^{ik_2(1-\cos\vartheta_c)z}$$

$$\times \int_0^1 dp\, p^{-1} G_1(p)^{-2} \exp\left[\frac{ik_3}{2zp}(x^2+y^2) + i(k_3 - 2k_1 + k_2)zp\right.$$

$$\left. + ik_2(\cos\vartheta_c - 1)zp\right]$$

$$\times \int_{-\infty}^{\infty} dx' \exp\left[-i\left\{k_2 \sin\vartheta_c + \frac{k_3 x}{zp}\right\}x' + \frac{iB_1(p)}{p}x'^2\right]$$

$$\times G_2(x',p)^{-1/2}\left[-\frac{B_1(p)}{p}G_2(x',p) - ik_2\right]^{-1/2}$$

$$\times \exp\left[\frac{i}{4G_2(x',p)}\left\{2ik_2 y_c + \frac{k_3 y}{zp}G_2(x',p)\right\}\left\{-\frac{B_1(p)}{p}G_2(x',p) - ik_2\right\}^{-1}\right]$$

$$\times \exp\left[-\frac{k_2}{G_2(x',p)}\left\{[x'\cos\vartheta_c - (z - zp - z_c)\sin\vartheta_c]^2\right.\right.$$

$$\left.\left. + y_c^2\right\}\right] \quad . \tag{27}$$

Within the limits imposed by the conditions (12), Eq. (27) is an exact result. It is not practical to use it in this form, however, because the integrals must be evaluated numerically. In order to reduce the computing time to acceptable levels, it was found to be necessary to perform at

least one additional analytical integration. This means that approximations must be introduced, and consequently the useful range of the results is determined by the accuracy of the approximations.

In order to facilitate the discussion of the effects of varying experimental parameters, it is convenient to use the ideal case of collinear, perfectly-overlapped beams as a comparison. The generated field strength for this ideal reference state, $E_3^{(0)}(\vec{r})$, can be obtained by setting $b_2 = b_1$ and $\vartheta_c = y_c = z_c = d = 0$ in Eq. (27). Noting that

$$G_2^{(0)}(p) = b_1 - 2i(1-p)z = G_1^*(p) \tag{28}$$

and defining

$$\Delta k = k_3 - 2k_1 + k_2 \tag{29}$$

and

$$Q(p) = [B_1(p) G_1^*(p) + i k_2 p]^{-1}, \tag{30}$$

we find

$$E_3^{(0)}(\vec{r}) = \left(\frac{\pi}{i}\right)^{1/2} k_c^2 A' e^{i(2k_1 - k_2)z} \int_0^1 \frac{dp}{p^{1/2}} G_1(p)^{-2} i^{-1} G_1^*(p)^{-1/2}$$

$$\times e^{i\Delta k z p} Q(p)^{1/2} \exp\left\{\frac{i k_3}{2zp}(x^2+y^2)\right\} \exp\left[-\frac{i k_3^2 y^2 G_1^*(p)}{4z^2 p} Q(p)\right]$$

$$\times \int_{-\infty}^{\infty} dx' \exp\left[-\frac{i k_3 x}{zp} x'\right] \exp\left[\frac{i x'^2}{p G_1^*(p) Q(p)}\right] \tag{31}$$

Eq. (21) can be used once again to obtain an expression which involves a single integration:

$$E_3^{(\omega)}(\vec{r}) = i\pi k_0^2 A' e^{i(2k_1 - k_2)z} \int_0^1 dp\, \mathcal{P}^{(\omega)}(p) \quad , \tag{32}$$

where

$$\mathcal{P}^{(\omega)}(p) = G_1(p)^{-2} e^{i\Delta k z p} Q(p) \times \exp\left[-\frac{k_3}{2z} \left\{ 2k_1 G_1^*(p) G_1(p)^{-1} + k_2 \right\} Q(p)(x^2 + y^2) \right] . \tag{33}$$

Eq. (27) can then be written in the form

$$E_3(\vec{r}) = i\pi k_0^2 A' e^{i(2k_1 - k_2)z} \int_0^1 dp\, \mathcal{P}^{(\omega)}(p)\, \mathcal{F}(p) \quad , \tag{34}$$

where

$$\begin{aligned} \mathcal{F}(p) = {} & i \left(\frac{i}{\pi} \right)^{1/2} p^{-1/2} Q(p)^{-1} \exp\left[i k_2 (1 - \cos\vartheta_c) z (1-p) \right. \\ & \left. + \frac{i k_3^2 G_1^*(p)}{4 z^2 p} Q(p)(x^2 + y^2) \right] \\ & \times \int_{-\infty}^{\infty} dx' \, G_2(x', p)^{-1/2} \left\{ B_1(p) G_2(x', p) + i k_2 p \right\}^{-1/2} \\ & \times \exp\left[\frac{i B_1(p)}{p} x'^2 - i \left\{ k_2 \sin\vartheta_c + \frac{k_3 x}{z p} \right\} x' \right. \\ & - \frac{ip}{4 G_2(x', p)} \left\{ 2 i k_2 y_c + \frac{k_3 y}{z p} G_2(x', p) \right\}^2 \left\{ B_1(p) G_2(x', p) + i k_2 p \right\}^{-1} \\ & \left. - \frac{k_2}{G_2(x', p)} \left\{ [x' \cos\vartheta_c - (z - zp - z_c)\sin\vartheta_c]^2 + y_c^2 \right\} \right] . \end{aligned} \tag{35}$$

Since all of the effects of variations from the ideal case are contained in the function $\mathcal{F}(p)$, Eq. (35) serves as

a starting point for systematic investigations of the effects of changing the experimental parameters. We examine several specific cases below.

B. Special Cases of Nonideality

1. Different beam sizes

We first consider the case in which the two laser beams are collinear, coplanar, and confocal, but have different diameters. The variable parameter is $\alpha_2 = 1 - b_2/b_1$, with all other parameters having their ideal values. Under these conditions,

$$G_2(x',\rho) = b_1(1-\alpha_2) - 2iz(1-\rho) = G_1^*(\rho) - b_1\alpha_2 \quad (36)$$

and Eq. (35) reduces to

$$\begin{aligned} \mathcal{F}(\rho) = {} & i\left(\frac{i}{\pi}\right)^{1/2} \rho^{-1/2} Q(\rho)^{-1} \left[G_1^*(\rho) - b_1\alpha_2\right]^{-1/2} \\ & \times \left[B_1(\rho)\left\{G_1^*(\rho) - b_1\alpha_2\right\} + ik_2\rho\right]^{-1/2} \\ & \times \exp\left[\frac{ik_3^2}{4z^2\rho}\left\{G_1^*(\rho)Q(\rho)(x^2+y^2) - \frac{y^2\left[G_1^*(\rho) - b_1\alpha_2\right]}{B_1(\rho)\left[G_1^*(\rho) - b_1\alpha_2\right] + ik_2\rho}\right\}\right] \\ & \times \int_{-\infty}^{\infty} dx' \exp\left[-\frac{ik_3x}{z\rho}x' - i\left\{-\frac{B_1(\rho)}{\rho} - \frac{ik_2}{G_1^*(\rho) - b_1\alpha_2}\right\}x'^2\right]. \end{aligned} \quad (37)$$

The integral in Eq. (37) is of the form of Eq. (21) and thus can be integrated exactly, giving

$$\mathcal{F}(\rho) = Q(\rho)^{-1}\left[B_1(\rho)\{G_1^*(\rho) - b_1\alpha_2\} + ik_2\rho\right]^{-1}$$

$$\times \exp\left[\frac{ik_3^2 G_1^*(\rho)}{4z^2\rho} Q(\rho)(x^2+y^2)\right.$$

$$\left. - \frac{ik_3^2}{4z^2\rho} \frac{\{G_1^*(\rho) - b_1\alpha_2\}(x^2+y^2)}{[B_1(\rho)\{G_1^*(\rho) - b_1\alpha_2\} + ik_2\rho]}\right] . \qquad (38)$$

2. Non-confocal beams

Next we treat the case of collinear, coplanar beams which are not confocal. Since the crossing angle is assumed to be zero, the interfocal distance is $d_f = z_c + d$. Here

$$G_2(x',\rho) = b_1 - 2iz(1-\rho) + 2i(z_c+d) = G_1^*(\rho) + 2id_f . \qquad (39)$$

If we make the identification $2id_f \longleftrightarrow -b_1\alpha_2$, $\mathcal{F}(\rho)$ can be written in a form which is identical to Eq. (37), so that the result of the integration can be written down immediately by analogy to Eq. (38):

$$\mathcal{F}(\rho) = Q(\rho)^{-1}\left[B_1(\rho)\{G_1^*(\rho) + 2id_f\} + ik_2\rho\right]^{-1}$$

$$\times \exp\left[\frac{ik_3^2 G_1^*(\rho)}{4z^2\rho} Q(\rho)(x^2+y^2)\right.$$

$$\left. - \frac{ik_3^2}{4z^2\rho} \frac{\{G_1^*(\rho) + 2id_f\}(x^2+y^2)}{[B_1(\rho)\{G_1^*(\rho) + 2id_f\} + ik_2\rho]}\right] . \qquad (40)$$

3. Offset beams

In this section we derive the function $\mathcal{F}(\rho)$ for collinear, confocal beams which have the same size and profile

but are offset by a distance y_c in a direction perpendicular to the direction of propagation. We have

$$G_2(x',p) = b_1 - 2iz(1-p) = G_1^*(p) , \tag{41}$$

so that $\mathcal{F}(p)$ becomes

$$\mathcal{F}(p) = i\left(\frac{i}{\pi}\right)^{1/2} p^{-1/2} Q(p)^{-1/2} G_1^*(p)^{-1/2}$$
$$\times \exp\left[\frac{ik_3^2 G_1^*(p)}{4z^2 p} Q(p)(x^2+y^2) - \frac{k_2 y_c^2}{G_1^*(p)} \right.$$
$$\left. - \frac{ip}{4G_1^*(p)} Q(p)\left\{ -4k_2 y_c^2 + \frac{4ik_2 k_3}{zp} G_1^*(p) y y_c \right.\right.$$
$$\left.\left. + \frac{k_3^2 y^2}{z^2 p^2} G_1^*(p)^2 \right\} \right]$$
$$\times \int_{-\infty}^{\infty} dx' \exp\left[-i\frac{k_3 x}{zp} x' - i\left\{ -\frac{B_1(p)}{p} - \frac{ik_2}{G_1^*(p)} \right\} x'^2 \right] .$$

(42)

We again see that the integral in Eq. (42) has the form of Eq. (21), so that the result can be written down immediately. Substitution and simplification leads to the result

$$\mathcal{F}(p) = \exp\left[-k_2 B_1(p) Q(p) y_c^2 + \frac{k_2 k_3}{z} Q(p) y y_c \right] . \tag{43}$$

4. Crossed beams

The most complex single-parameter variation is that

due to the crossing angle ϑ_c. Assuming all of the other parameters to have their ideal values, we have

$$G_2(x',p) = b_1 - 2ik(1-p)\cos\vartheta_c - 2ix'\sin\vartheta_c$$

$$= \Gamma(p) - 2ix'\sin\vartheta_c \quad . \tag{44}$$

The expression for $\mathcal{F}(p)$ then becomes

$$\mathcal{F}(p) = i\left(\frac{i}{\pi}\right)^{1/2} p^{-1/2} Q(p)^{-1} \exp\left[ik_2(1-\cos\vartheta_c)z(1-p)\right.$$

$$\left. + \frac{ik_3^2 G_1^*(p)}{4z^2 p} Q(p)(x^2+y^2)\right]$$

$$\times \int_{-\infty}^{\infty} dx' \left[\Gamma(p) - 2ix'\sin\vartheta_c\right]^{-1/2} \left[B_1(p)\left\{\Gamma(p) - 2ix'\sin\vartheta_c\right\} + ik_2 p\right]^{-1/2}$$

$$\times \exp\left\{i\frac{B_1(p)}{p}x'^2 - i\left\{k_2\sin\vartheta_c + \frac{k_3 x}{zp}\right\}x'\right.$$

$$- \frac{ik_3^2 y^2}{4z^2 p} \frac{\left\{\Gamma(p) - 2ix'\sin\vartheta_c\right\}}{\left[B_1(p)\left\{\Gamma(p) - 2ix'\sin\vartheta_c\right\} + ik_2 p\right]}$$

$$\left. - \frac{k_2\left[x'\cos\vartheta_c - z(1-p)\sin\vartheta_c\right]^2}{\Gamma(p) - 2ix'\sin\vartheta_c}\right] \quad . \tag{45}$$

The integral in Eq. (44) cannot be evaluated exactly because of its complexity, so it is necessary to resort to an approximate method. Since the crossing angles of experimental interest are typically small for gases, a natural

choice is to make the assumptions

$$\left| \frac{2i\chi' \sin\vartheta_c}{\Gamma(p)} \right| \ll 1 \tag{46a}$$

and

$$\left| \frac{2i\chi' B_1(p) \sin\vartheta_c}{B_1(p)\Gamma(p) + ik_2 p} \right| \ll 1 \tag{46b}$$

These conditions are obviously satisfied for sufficiently small χ'. However, the integral over χ' covers the entire axis $(-\infty,\infty)$, so that they cannot be satisfied uniformly if $\vartheta_c \neq 0$. Fortunately, there are other terms in the integrand which decrease exponentially as $|\chi'|$ increases, so that the conditions (46) can be assumed to hold in those regions where the integrand makes significant contributions to the value of the integral. In practice, the range of validity of Eqs. (46) can be determined readily by a few simple numerical computations.

When the conditions (46) are satisfied, the terms of the form $(1 - \alpha\chi')^{-n}$, where $n = \frac{1}{2}$ or 1, in Eq. (45) can be represented by truncated series expansions. Numerical experimentation showed that for crossing angles within the range of experimental interest ($\vartheta_c \lesssim 3^\circ$), the linear approximation

$$(1 - \alpha\chi')^{-n} \approx 1 + n\alpha\chi' \tag{47}$$

resulted in errors no larger than about 1%. This was verified in test cases by computing the corrections due to the

quadratic terms.

Defining

$$A_F = i\left(\frac{i}{\pi}\right)^{1/2} p^{-1/2} Q(p)^{-1} \exp\left[ik_2(1-\cos\vartheta_c)z(1-p)\right.$$
$$\left. + \frac{ik_3^2 G_1^*(p)}{4z^2 p} Q(p)(x^2+y^2)\right] , \tag{48}$$

$$a = 2i\sin\vartheta_c , \tag{49}$$

and

$$\Gamma'(p) = \Gamma(p) + \frac{ik_2 p}{B_1(p)} , \tag{50}$$

we can write Eq. (45) in the more compact form

$$\mathcal{F}(p) = A_F B_1(p)^{-1/2} \int_{-\infty}^{\infty} dx' \left[\Gamma(p) - ax'\right]^{-1/2} \left[\Gamma'(p) - ax'\right]^{-1/2}$$
$$\times \exp\left[i\frac{B_1(p)}{p} x'^2 - i\left\{k_2\sin\vartheta_c + \frac{k_3 x}{zp}\right\} x' \right.$$
$$- \frac{ik_3^2 y^2}{4z^2 p B_1(p)} \left\{\Gamma(p) - ax'\right\}\left\{\Gamma'(p) - ax'\right\}^{-1}$$
$$\left. - \frac{k_2\left[x'\cos\vartheta_c - z(1-p)\sin\vartheta_c\right]^2}{\Gamma(p) - ax'} \right] . \tag{51}$$

Then, using Eq. (47),

$$\mathcal{F}(p) \approx A_2 B_1(p)^{-1/2}\{\Gamma(p)\Gamma'(p)\}^{-1/2}$$

$$\times \exp\left\{-\frac{ik_3^2 y^2 \Gamma(p)}{4z^2 p B_1(p)\Gamma'(p)} - \frac{k_2 z^2 (1-p)^2 \sin^2\vartheta_c}{\Gamma(p)}\right\}$$

$$\times \int_{-\infty}^{\infty} dx' \left(1 + \frac{ax'}{2\Gamma'(p)} + \frac{ax'}{2\Gamma(p)}\right) \exp\left(-\frac{2ik_2}{\Gamma(p)^2}\sin\vartheta_c \cos^2\vartheta_c x'^3\right)$$

$$\times \exp\left[\left\{i\frac{B_1(p)}{p} - \frac{k_2}{\Gamma(p)}\cos^2\vartheta_c + \frac{4ik_2 z(1-p)\sin^2\vartheta_c\cos\vartheta_c}{\Gamma(p)^2}\right\}x'^2\right.$$

$$+\left\{-ik_2\sin\vartheta_c - \frac{ik_3 x}{2p} + \frac{2k_2 z(1-p)}{\Gamma(p)}\sin\vartheta_c\cos\vartheta_c\right.$$

$$-\frac{k_3^2 y^2 \sin\vartheta_c}{2z^2 p\,\Gamma'(p)}\left(1 - \frac{\Gamma(p)}{\Gamma'(p)}\right)$$

$$\left.\left. - \frac{2ik_2 z^2 (1-p)^2}{\Gamma(p)^2}\sin^3\vartheta_c\right\} x'\right] . \qquad (52)$$

By expanding the last exponential term in the integrand of Eq. (52), it is possible to reduce $\mathcal{F}(p)$ to the form

$$\mathcal{F}(p) \approx A_1 \int_{-\infty}^{\infty} dx' (1 + \lambda_1 x' + \lambda_3 x'^3) \exp(-\mu_2 x'^2 - \mu_1 x') , \qquad (53)$$

where

$$A_1 = A_2 B_1(p)^{-1/2}\{\Gamma(p)\Gamma'(p)\}^{-1/2} \exp\left\{-\frac{ik_3^2 y^2 \Gamma(p)}{4z^2 p B_1(p)\Gamma'(p)}\right.$$
$$\left. - k_2\Gamma(p)^{-1} z^2 (1-p)^2 \sin^2\vartheta_c\right\} \qquad (54)$$

$$\lambda_1 = i \sin\vartheta_c \left(\frac{1}{\Gamma'(p)} + \frac{1}{\Gamma(p)} \right) \tag{55}$$

$$\lambda_3 = -\frac{2 i k_2}{\Gamma(p)^2} \sin\vartheta_c \cos^2\vartheta_c \tag{56}$$

$$\begin{aligned} \mu_1 = {} & -i k_2 \sin\vartheta_c - \frac{i k_3 x}{2p} + \frac{2 k_2 z (1-p)}{\Gamma(p)} \sin\vartheta_c \cos\vartheta_c \\ & - \frac{k_3^2 y^2 \sin\vartheta_c}{2 z^2 p \Gamma'(p)} \left(1 - \frac{\Gamma(p)}{\Gamma'(p)} \right) - \frac{2 i k_2 z^2 (1-p)}{\Gamma(p)^2} \sin^3\vartheta_c \end{aligned} \tag{57}$$

$$\mu_2 = i \frac{B_1(p)}{p} - \frac{k_2}{\Gamma(p)} \cos^2\vartheta_c + \frac{4 i k_2 z (1-p)}{\Gamma(p)^2} \sin^2\vartheta_c \cos\vartheta_c \,. \tag{58}$$

The integral in Eq. (53) can be evaluated by the general formula

$$\begin{aligned} & \int_{-\infty}^{\infty} \sum_{m=0}^{M} \lambda_m x^m \exp\left(-\mu_1 x - \mu_2 x^2\right) dx \\ & = \left(\frac{\pi}{\mu_2} \right)^{1/2} e^{\mu_1^2 / 4\mu_2} \sum_{m=0}^{M} (-1)^m m! \, \lambda_m \\ & \quad \times \sum_{\substack{\kappa=0 \\ (\kappa \text{ even})}}^{m} \frac{\mu_1^{(m-\kappa)} (2\mu_2)^{\kappa/2 - m}}{\kappa! \, (m-\kappa)!} \,, \end{aligned} \tag{59}$$

to obtain

$$f(p) \approx A_1 \left[1 - \lambda_1 \left(\frac{\mu_1}{2\mu_2} \right) - \lambda_3 \left(\frac{\mu_1}{2\mu_2} \right)^2 \left(\frac{\mu_1}{2\mu_2} + \frac{3}{\mu_1} \right) \right] . \tag{60}$$

5. Simultaneously crossed and offset beams

In an actual experimental situation, several of the parameters treated above may vary simultaneously. To illustrate the treatment of multivariate beam characteristics,

we will consider the case of laser beams with a crossing angle ϑ_c and simultaneous lateral offset y_c. In this case we have

$$
\begin{aligned}
\mathcal{F}(p) = i\left(\frac{i}{\pi}\right)^{1/2} p^{-1/2}\, Q(p)^{-1} \exp\Big[& i k_2 z (1-p)(1-\cos\vartheta_c) \\
& + i k_3^2 G_1^*(p)(4z^2 p)^{-1} Q(p)(x^2+y^2)\Big] \\
\times \int_{-\infty}^{\infty} dx'\, G_2(x',p)^{-1/2} & \left[B_1(p) G_2(x',p) + i k_2 p\right]^{-1/2} \\
\times \exp\Bigg[& \frac{i B_1(p)}{p} x'^2 - i k_2 x' \sin\vartheta_c - \frac{i k_3 x x'}{z p} \\
& - \frac{i p}{4 G_2(x,y)} \frac{\left\{2 i k_2 y_c + \frac{k_3 y}{z p} G_2(x',p)\right\}^2}{\left\{B_1(p) G_2(x',p) + i k_2 p\right\}} \\
& - \frac{k_2}{G_2(x',p)} \left\{\left[x' \cos\vartheta_c - z(1-p)\sin\vartheta_c\right]^2 + y_c^2\right\} \Bigg] ,
\end{aligned}
\tag{61}
$$

where $G_2(x',p)$ is again given by Eq. (44).

Although Eq. (64) is rather complicated, it differs from Eq. (45) only in the terms containing y_c. In order to take advantage of this similarity, we write

$$\mathcal{F}(p) = i\left(\frac{i}{\pi}\right)^{1/2} p^{-1/2}\, Q(p)^{-1} \exp\Big[i k_2 z (1-p)(1-\cos\vartheta_c)$$

$$+ i k_3^2 G_1^*(p)(4z^2 p)^{-1} Q(p)(x^2+y^2)\Big]$$

$$\times \int_{-\infty}^{\infty} dx'\, G_2(x',p)^{-1/2} \left[B_1(p) G_2(x',p) + i k_2 p\right]^{-1/2}$$

$$\times \exp\Bigg[\frac{i B_1(p)}{p} x'^2 - i k_2 x' \sin\vartheta_c - \frac{i k_3 x x'}{2p}$$

$$- i \frac{k_3^2 y^2}{4z^2 p} G_2(p) \left\{ B_1(p) G_2(x',p) + i k_2 p \right\}^{-1}$$

$$- k_2 G_2(x',p)^{-1} \left[x' \cos\vartheta_c - z(1-p)\sin\vartheta_c \right]^2 \Bigg]$$

$$\times \exp\Bigg[\left\{ \frac{i p k_2^2 y_c^2}{G_2(x',p)} + \frac{k_2 k_3 y y_c}{z} \right\} \left\{ B_1(p) G_2(x',p) + i k_2 p \right\}^{-1}$$

$$- k_2 y_c^2 G_2(x',p)^{-1} \Bigg] , \qquad (62)$$

where the last exponential term contains the entire effect of the offset y_c. Making use of Eqs. (44) and (50), this term can be written in the form

$$\mathcal{F}_{co} = \exp\left[\frac{\left\{ i p k_2^2 y_c^2 \left(\Gamma(p) - a x'\right)^{-1} + \frac{k_2 k_3}{z} y y_c \right\}}{B_1(p)\left(\Gamma(p) - a x'\right) + i k_2 p} - \frac{k_2 y_c^2}{\Gamma(p) - a x'} \right] \qquad (63)$$

The expansion of Eq. (47) can now be used again, reducing Eq. (63) to

$$\mathcal{F}_{co} \approx \exp\left[\frac{ip k_2^2 y_c^2}{B_1(p)\Gamma(p)\Gamma'(p)} + \frac{k_2 k_3 y y_c}{2B_1(p)\Gamma'(p)} - \frac{k_2 y_c^2}{\Gamma(p)}\right]$$

$$\times \exp\left\{\left[\frac{ip}{B_1(p)\Gamma(p)\Gamma'(p)}\left(\frac{1}{\Gamma(p)} + \frac{1}{\Gamma'(p)}\right)k_2 y_c + \frac{k_3 y}{2B_1(p)\Gamma'(p)^2}\right.\right.$$

$$\left.\left. - \frac{y_c}{\Gamma(p)^2}\right] k_2 y_c a x'\right\} . \qquad (64)$$

Therefore, $\mathcal{F}(p)$ can be obtained directly from Eq. (60) by making the replacements

$$A_1 \longrightarrow A_1 \exp\left[\left\{\frac{ip k_2 y_c}{B_1(p)\Gamma(p)\Gamma'(p)} + \frac{k_3 y}{2B_1(p)\Gamma'(p)} - \frac{y_c}{\Gamma(p)}\right\} k_2 y_c\right] \qquad (65)$$

and

$$\mu_1 \longrightarrow \mu_1 - \left[\frac{ip}{B_1(p)\Gamma(p)\Gamma'(p)}\left(\frac{1}{\Gamma(p)} + \frac{1}{\Gamma'(p)}\right)k_2 y_c + \frac{k_3 y}{2B_1(p)\Gamma'(p)^2} - \frac{y_c}{\Gamma(p)^2}\right] k_2 y_c a \qquad (66)$$

III. CALCULATION OF THE RELATIVE POWER GENERATION

The energy flux generated at a given point in space is proportional to the squared magnitude of the electric field strength as given by Eq. (32) or Eq. (34). Integrating over the cross section of the cell then gives the total power generation at the frequency $\omega_3 = 2\omega_1 - \omega_2$. Alternatively,

it is possible to compute the profile of the generated signal over the cross section of the cell or to follow the buildup of the signal along the direction of propagation of the laser beams.

The primary interest here is in the performance of the system relative to the ideal case (collinear, confocal beams with identical profiles). This case is somewhat simplified by the cancellation of the common multiplicative factors in Eqs. (32) and (34). The major computational difficulty is the multiple numerical integration which must be performed in order to obtain the relative power generation.

The numerical computations were performed on the ASC system at the Naval Research Laboratory. The integrals were performed by straightforward application of Weddle's Rule (9). The only innovation was the inclusion of a variable step size feature to increase the speed of the integration routine in regions where the integrand is slowly varying. This modification was found to be absolutely necessary in order to obtain acceptable accuracy at reasonable cost. Typical computation times were of the order of 30 seconds of CPU time for each set of experimental parameters. A more detailed description of the computational procedure is given in the Appendix.

IV. RESULTS

A. Different Beam Diameters

Figure 2 shows the results of varying the parameter $\alpha_2 = 1 - b_2/b_1$. The negative values correspond to the case in which the waist diameter of the ω_2 beam is larger than that of the ω_1 beam, while the positive values result from tighter focussing of the ω_2 beam. All of the other experimental parameters are held constant.

It is quite clear from Figure 2 that it is possible to realize substantial relative power gains by tightening the focus of the ω_2 beam relative to the ω_1 beam. There are experimental limitations on the extent to which this can be achieved *in practice*, but power enhancements of as much as 50% (requiring $b_2 \simeq 0.65\, b_1$) seem quite reasonable.

B. Non-confocal Beams

The variation in signal power which results from a relative longitudinal displacement of the foci of the two laser beams is illustrated by Figure 3. Positive values of d_f correspond to shifts of the ω_2 focus in the direction of propagation. For the parameter values chosen here, the results indicate that the power generated by collinear beams can be enhanced by about 9% by displacing the focus of the ω_2 beam by 0.04 cm in the direction of propagation.

C. Offset Beams

Figure 4 shows the effect of lateral displacements of two collinear, confocal beams with identical profiles. The

relative total power generation is plotted as a function of the offset parameter $\alpha_3 = y_c / b_1$, where y_c is the actual offset and b_1 is the reduced beam radius defined by Eq. (2). Although the power generation drops sharply with increasing α_3 for $\alpha_3 \gtrsim 0.01$, the model predicts a slight increase in power for smaller displacements. The maximum occurs at $y_c \approx 0.005\, b_1$. An important practical consequence of this result is the fact that it is not necessary to achieve precise collinearity in the alignment of an experimental CARS system.

D. Crossed Beams

Figure 5 is a plot of the relative total power generation as a function of the crossing angle for two non-collinear beams which cross at their focal points. As expected, there is a loss of power generation when the beams are crossed. However, the magnitude of the decrease is not as large as might be anticipated. The model predicts that the beams can be crossed at angles as large as $\sim 2.5^\circ$ with no more than 50% power loss. In many cases this is quite adequate to obtain a useful spatial separation of the CARS output beam.

E. Crossed and Offset Beams

As an example of the simultaneous variation of more than one experimental parameter, Figure 6 displays the results of variations of the crossing angle ϑ_c and the offset parameter $\alpha_3 = y_c / b_1$. It can be seen that the effects of

the two parameters are essentially independent for small variations, although there is a slight increase in the optimum offset of the two beams as the crossing angle increases. The convergence and eventual crossing of the curves is of little practical consequence, since the corresponding parameter values are either outside the region of experimental interest, near the limits of validity of the model, or both.

F. Longitudinal Growth of the CARS Signal

It is easy to modify the basic computer program to calculate the accumulated power over the cross section of the cell as a function of the longitudinal distance from the focal point in the direction of propagation of the primary beam, ω_1. The center of the ω_1 beam is assumed to propagate along the centerline of the cell. This computation serves to identify the active volume of the cell in which the major fraction of the signal power is generated.

Figure 7 shows the signal buildup starting from the focal point and proceeding in the direction of propagation. Results are plotted both for collinear beams and for a crossing angle of 0.01 radians. The units of power are arbitrary, with the reference level being chosen as the cumulative power generated by collinear beams at the focal point.

It is clear from the figure that most of the power is generated within a very narrow band ($\sim$0.5 cm) near the center of the cell. This is a graphic demonstration of the increased spatial resolution which can be obtained by tight

focussing of the laser beams. The growth of the signal is roughly linear through the active band. As might have been anticipated from the results shown in Figure 3, the point of maximum signal generation is displaced from the focal point in the direction of propagation.

Interestingly, the model predicts a slightly enhanced rate of signal generation in the active zone for the crossed beams relative to the collinear case. The loss of signal power resulting from the beam crossing is thus attributed to increased attenuation as the beams pass through the remainder of the sample cell. Although a relative improvement in spatial resolution is an expected result of the beam crossing, one might expect to observe a noticeable loss of absolute signal power for an angle as great as 0.01 radian.

G. Spatial Profile of the CARS Beam

The basic computer program can also be modified readily to permit the calculation of the generated radiation flux as a function of the lateral position. This modified program was used to determine the profile of the generated signal as it emerges from the exit face of the sample cell. Calculations were performed for collinear beams as well as for a crossing angle of 0.035 radian ($\sim 2^{\circ}$), and the results produced no surprises. With crossed beams, the center of the CARS beam emerged at the point predicted by the simple vector addition of propagation vectors and there appeared to

be little or no distortion of the beam shape. At the end of the cell (5 cm beyond the focal point of the primary laser beams) the CARS beam was displaced from the center of the ω_1 beam by 0.08 cm.

V. SUMMARY

A computer model has been developed to predict the relative signal power generated by the CARS process under a variety of experimental conditions. It has been demonstrated that useful results can be obtained at modest cost and that the model can be used to aid the selection of optimum experimental parameters. In particular, the model calculations indicate that precise alignment of the laser beams is not a critical requirement. The predicted power losses which result from small lateral displacements or shifts of the focal points are relatively modest. Furthermore, it appears that the laser beams can be crossed to achieve spatial filtering of the CARS signal without excessive signal attenuation.

The primary limitation of the model described in this paper is its restriction to laser beams with Gaussian profiles. Many current CARS experiments involve the use of beams with substantially different forms. For example, the so-called "unstable resonator" (10) generates a laser output with a cross section in the shape of a doughnut. The result is a more uniform power distribution which can produce a larger total CARS signal without saturating the active medium (11). In order to keep pace with these experimental developments, the theoretical model must be extended to laser beams with arbitrary cross sections. It is hoped that this paper will stimulate further work on the generation of higher-order Raman signals by non-Gaussian laser beams.

VI. ACKNOWLEDGMENTS

The author is indebted to Dr. Albert Harvey for suggesting the problem and for providing support and encouragement, to Dr. Walter Shaub for many helpful discussions and for preparing the figures, and to Dr. Stephen Lemont for his experimental insights.

VII. REFERENCES

1. A. B. Harvey, J. R. McDonald and W. M. Tolles, "Analytical Applications of a New Spectroscopic Tool - Coherent Anti-Stokes Raman Spectroscopy," in Progress in Analytical Chemistry (I. L. Simmons and G. W. Ewing, Eds.), Plenum Press, New York, 1977, Vol. 8, p. 211.

2. For a review and list of references, see W. M. Tolles, J. W. Nibler, J. R. McDonald and A. B. Harvey, Appl. Spec., 31, 253 (1977).

3. P. D. Maker and R. W. Terhune, Phys. Rev. 137, A801 (1965).

4. G. C. Bjorklund, "Effects of Focusing on Third-Order Nonlinear Processes in Isotropic Media", Bell Laboratories TM 74-1313-23 (1974).

5. H. Kogelnik and T. Li, Proc. IEEE 54, 1312 (1966).

6. N. Bloembergen, "Nonlinear Optics", W. A. Benjamin, New York, 1965.

7. D. A. Kleinman, Phys. Rev. 128, 1761 (1962).

8. A. Messiah, "Quantum Mechanics", John Wiley & Sons, New York, 1961, Vol. 1.

9. Z. Kopal, "Numerical Analysis", Chapman & Hall, London, 1961, 2nd Ed., p. 413.

10. A. E. Siegman, Proc. IEEE 53, 277 (1965).

11. R. L. Herbst, H. Komine and R. L. Byer, Optics Comm. 21, 5 (1977).

APPENDIX

Details of the Computational Program

The electric field strength $E_3(\vec{r})$ of the CARS signal at the point $\vec{r}$ (in the coordinate system defined by Figure 1) is given by Eq. (32) for the ideal case, and by Eq. (34) for the more general case. The relative signal power generated at the point $\vec{r}$ is then given by

$$\Pi_{rel}(\vec{r}) = \frac{|E_3(\vec{r})|^2}{|E_3^{(0)}(\vec{r})|^2} = \frac{\left|\int_0^1 d\rho\, \mathcal{P}^{(0)}(\rho)\, \mathcal{F}(\rho)\right|^2}{\left|\int_0^1 d\rho\, \mathcal{P}^{(0)}(\rho)\right|^2} \quad , \tag{A-1}$$

where $\mathcal{P}^{(0)}(\rho)$ is defined by Eq. (33) and $\mathcal{F}(\rho)$ by Eq. (35).

The total relative power generation $P_{rel}(z)$ at the longitudinal position z is obtained by integrating over the area of the cell:

$$P_{rel}(z) = \int_{cell} dA\, \Pi_{rel}(\vec{r}) \quad . \tag{A-2}$$

The resulting three-fold integral was evaluated numerically on the ASC computing system at the Naval Research Laboratory. The FORTRAN program was constructed in such a way as to permit easy modification for the purpose of computing transverse power profiles, longitudinal buildup of the signal, etc. The program structure consists of the main program plus a set of three nested subroutines, as outlined below:

Main Program - initializes data and computes integral over ϑ

Subroutine RINT - computes integral over R

Subroutine PINT - computes integral over p

Subroutine PGEN - computes integrands

With this program structure, it is very easy to modify the computations to deal with different combinations of experimental parameters. Since all of the effects of deviations from the ideal case are contained in the factor $\mathcal{F}(\rho)$ in Eq. (A-1), it is only necessary to modify the subroutine PGEN. One exception was the computation of the transverse profile of the generated signal, which required minor alterations to the main program and the subroutine RINT.

Because of the three-fold numerical integration, it was necessary to exercise some care in setting up the integration routines in order to keep the computing time within reasonable bounds. The integrals were evaluated by Weddle's Rule (9), which appeared to be a satisfactory compromise between maximum accuracy and reasonable time requirements. In order to keep the computational times within acceptable limits, it was found to be necessary to use a variable integral step size.

The most effective strategy for minimizing computational time is to use an automatic criterion for selecting the step size in accordance with the rate of change of the integrand. Although some experimentation was performed with

such a procedure, it was found not to be worth the additional programming effort for the parameter combinations considered here. Instead, the integrands were plotted out for a sampling of the variable parameters, and a set of integral steps was selected to optimize the least favorable case. The same integration subintervals and step sizes were then used for all parameter combinations. This procedure resulted in reductions of computing time by as much as a factor of 100 in comparison with fixed-step-size calculations of the same accuracy. Since this brought the total computing requirements within acceptable limits, no attempts were made to achieve additional economies. In the "production" version of the program, a single step size was used for the integral over ϑ, while the integral over R was divided into 2 subintervals and the integral over the variable p was divided into 3 subintervals.

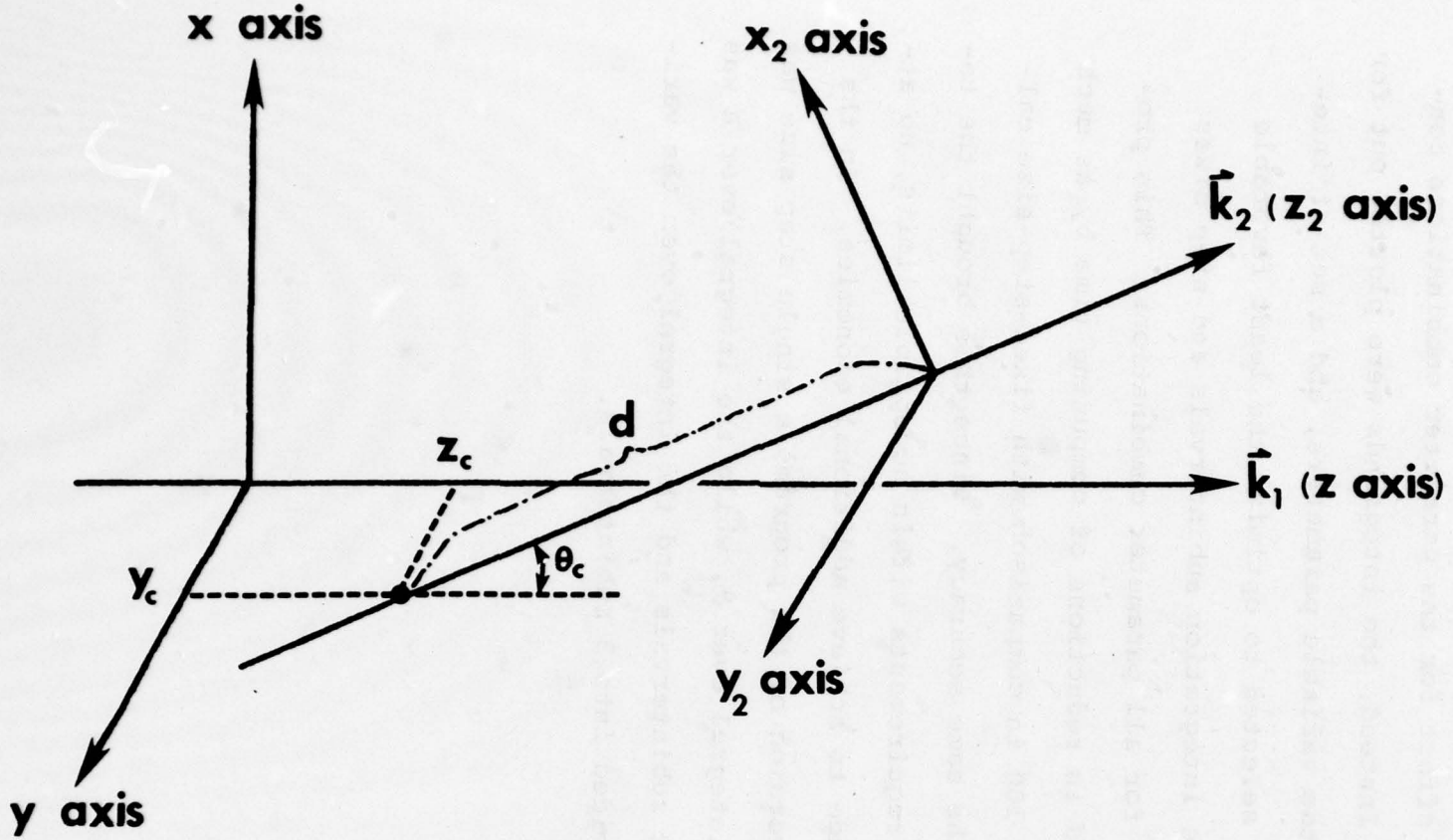

Fig. 1 — Coordinate system used to describe the beam crossing geometry

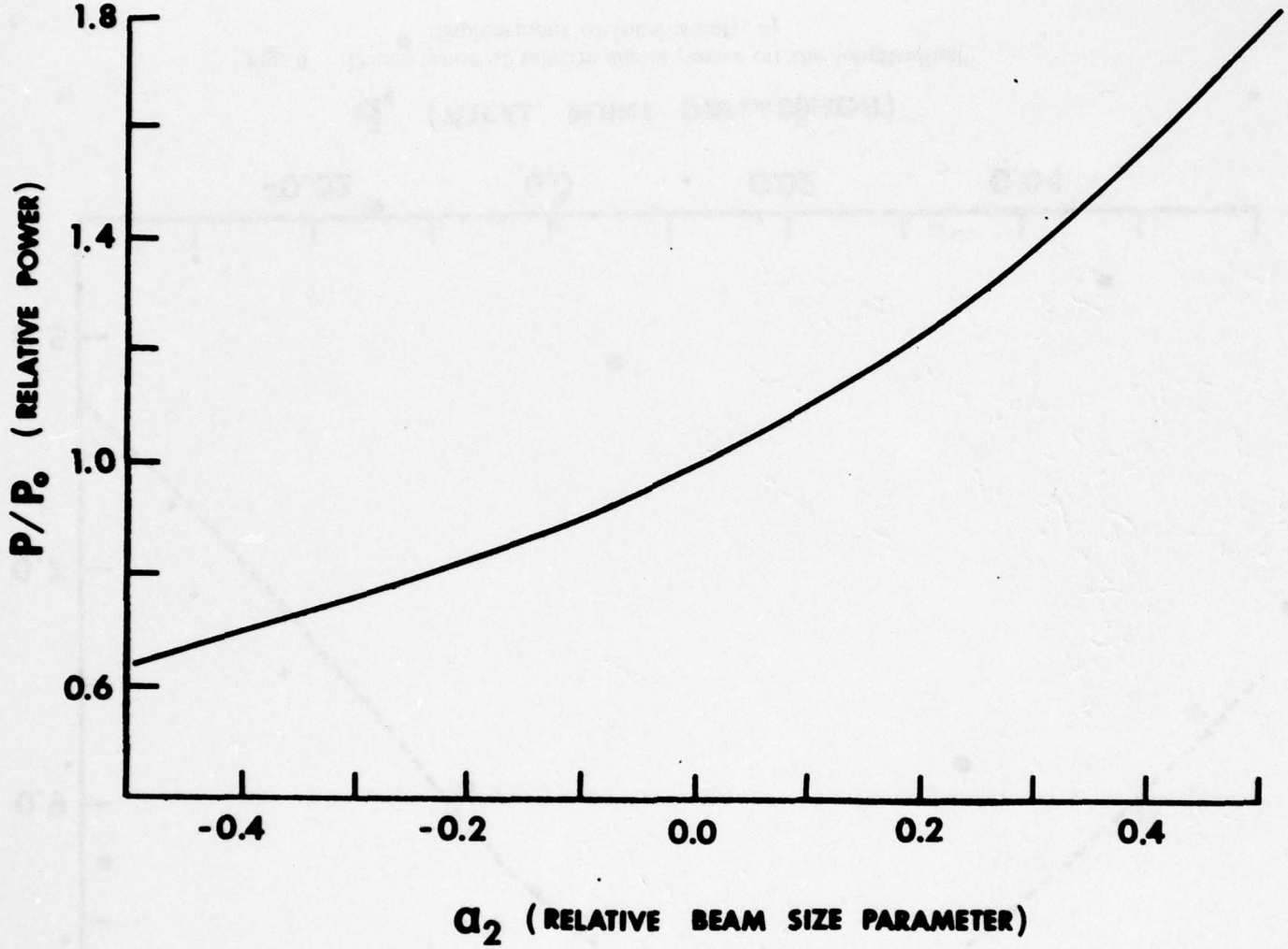

Fig. 2 — Dependence of relative signal power on the parameter $\alpha_2 = 1 - b_2/b_1$, where b_2/b_1 is the ratio of beam waist diameters

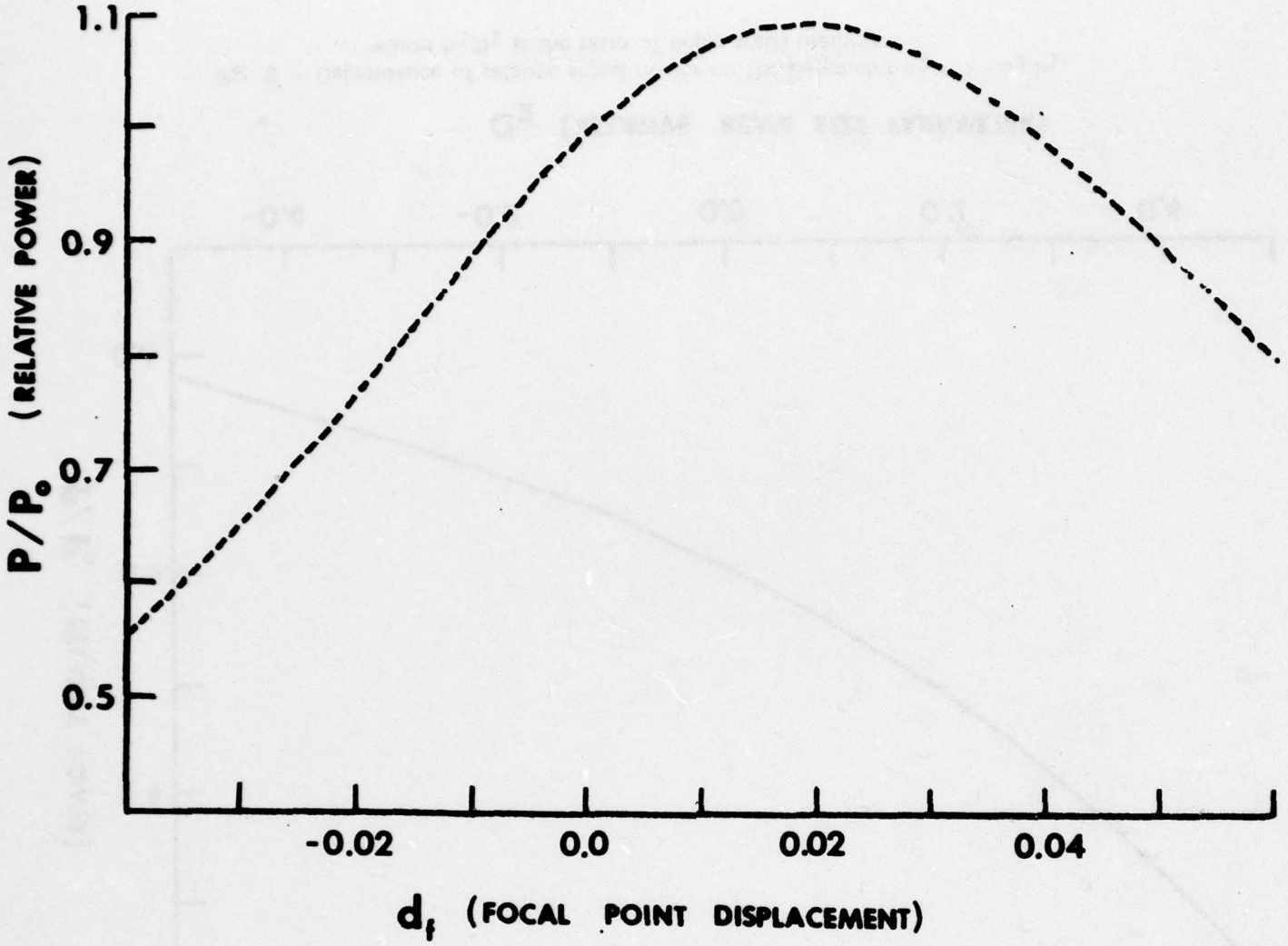

Fig. 3 — Dependence of relative signal power on the longitudinal displacement of focal points, d_f

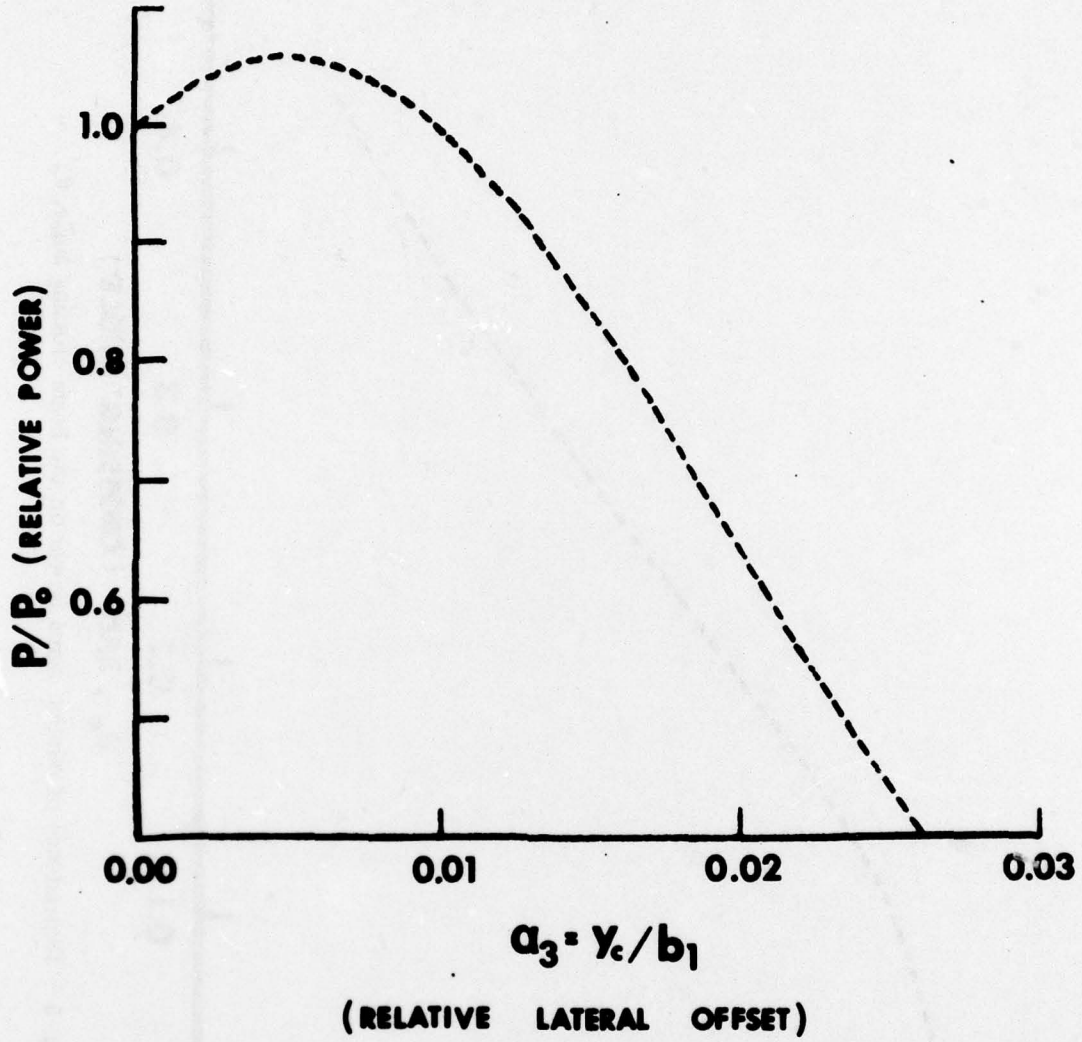

Fig. 4 — Dependence of relative signal power on the lateral displacement of the laser beams, $\alpha_3 = y_c/b_1$

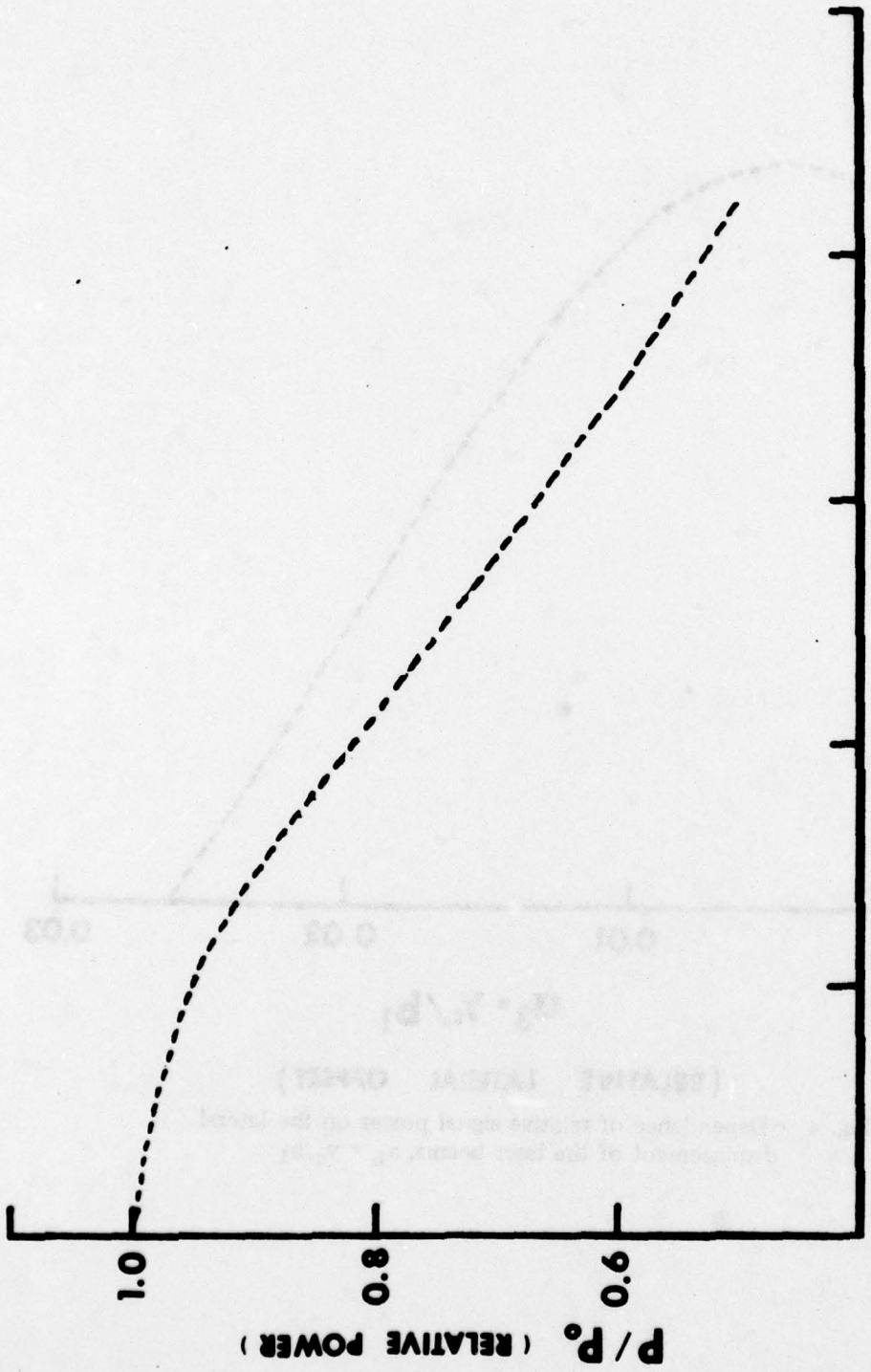

Fig. 5 — Dependence of relative signal power on the beam crossing angle, θ_c

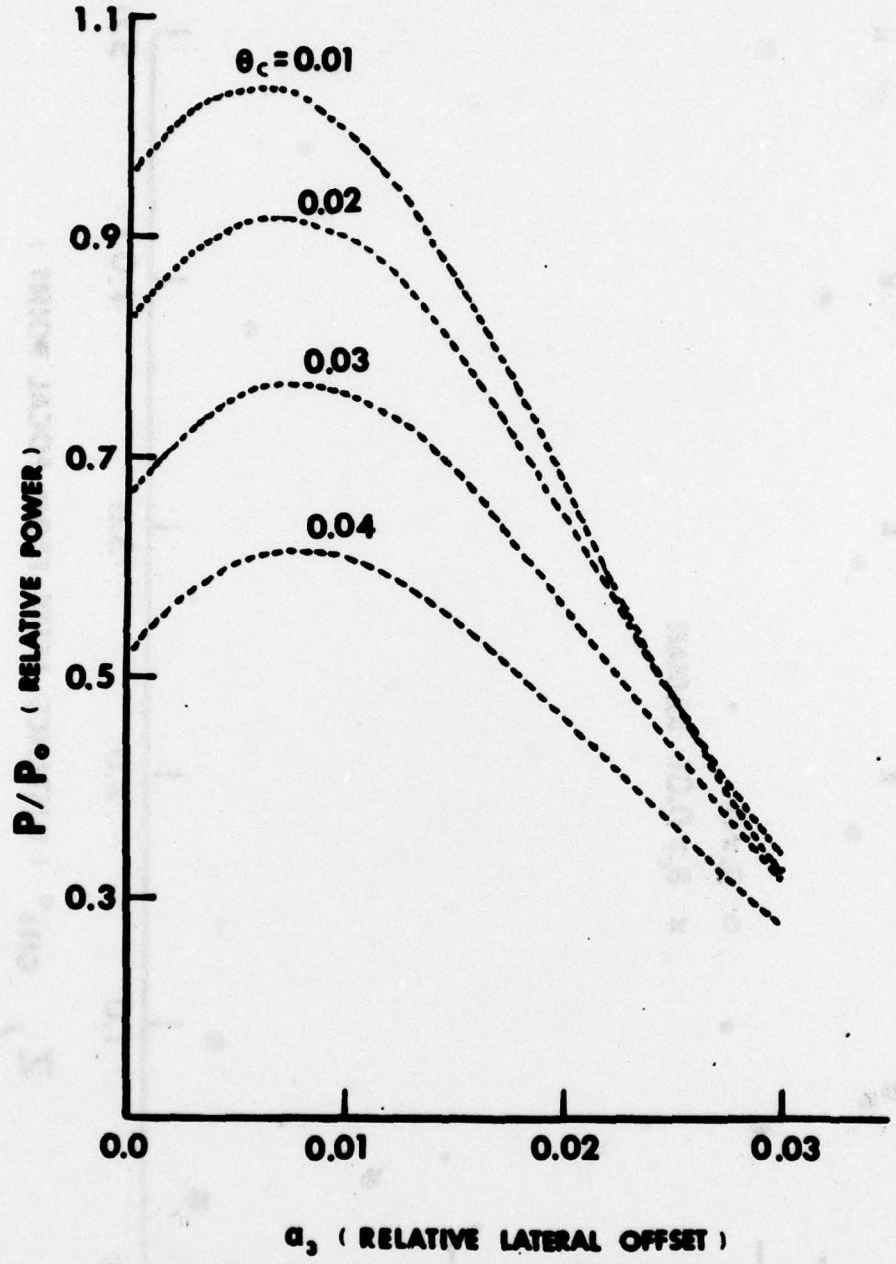

Fig. 6 — Dependence of relative signal power on simultaneous variations of the crossing angle, θ_c, and the lateral displacement, $\alpha_3 = y_c/b_1$

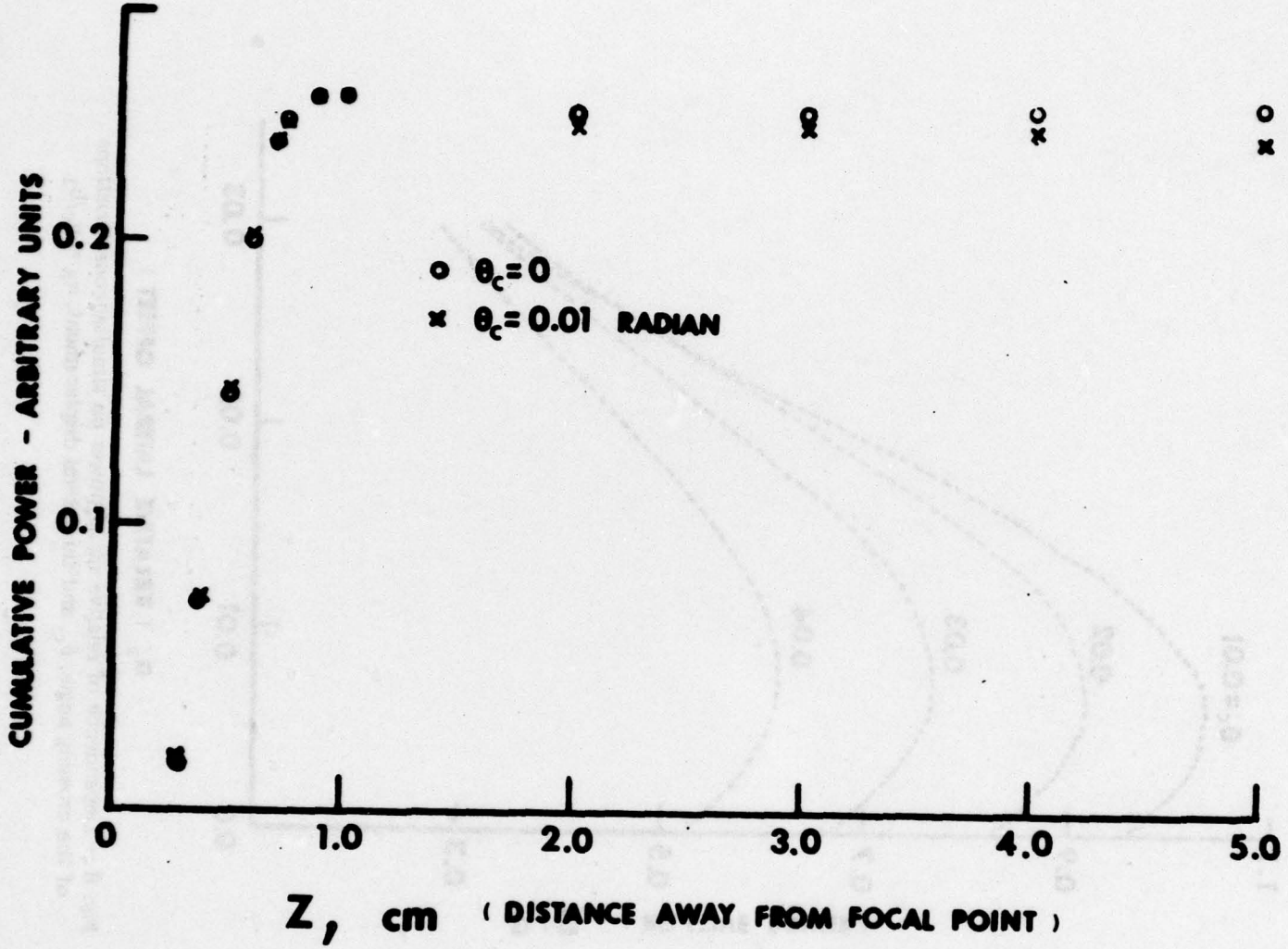

Fig. 7 — Longitudinal growth of the CARS signal for collinear laser beams (o) and for beams crossed at an angle of 0.01 radian (x)